Satellite Inversion of Cloud and Radiation Quantities Using ScaRaB Visible and Shortwave Measurements

F.-L. Chang, Z. Li, and A. P. Trishchenko
Canada Centre for Remote Sensing
Ottawa, Ontario, Canada

Introduction

Cloud and radiation both play important roles in governing the climate (Wielicki et al. 1995). A good knowledge of the two variables and their interactions can help model the climate. Although operational meteorological satellites have provided a wealth of observations, the inversion from observed radiances to physical quantities, such as the cloud optical properties and top-of-atmosphere (TOA) shortwave (SW) albedo, is still not fully resolved. While cloud properties can be inferred from narrowband measurements (e.g., Rossow and Schiffer 1991), SW TOA albedos are better derived with broadband measurement programs, like the Earth Radiation Budget Experiment (ERBE) or the Scanner for Radiation Budget (ScaRaB). These programs were, however, only experimental and of limited time. To fill gaps in the time record, narrowband data were also used to estimate the broadband quantities (Cess and Potter 1986).

To derive TOA albedos from satellite observations requires a process of angular correction. This angular correction for converting reflectance to albedo currently relies on the use of ERBE angular dependence model (ADM) (Suttles et al. 1988). For a given surface type, ERBE ADMs are differentiated only by four categories of cloud coverage. Clearly, for clouds with varieties of optical depths and microphysics, accurate inversion of angular correction demanded more sophisticated ADMs (Wielicki et al. 1996).

In this study, we used one-year (March 1994 to February 1995) ScaRaB visible and SW radiance measurements to evaluate the inversion of cloud and radiation quantities with prevalent models. The evaluation includes the retrieval of cloud optical depth from visible radiance, the inversion of radiances from visible to SW, and the angular conversion of SW reflectance to TOA albedo using ERBE ADM.

Data Analysis

The ScaRaB is a four-channel cross-track scanning radiometer with the field of view of ~60 km at nadir (Kandel et al. 1998). The four channels include two narrowbands (visible and infrared) and two broadbands (SW and total), but only the visible (0.55 μm to 0.65 μm) and SW (0.2 μm to 4 μm) observations were used in this study. The data products used here are the ScaRaB A2 level, which is directly comparable to the ERBE Processed Archival Tapes (PAT or S-8).

In the data analysis, observations over oceans between 60°S–60°N were sampled every 250 km along the satellite track. Within each 250-km sampled region, the visible and SW radiances observed from scenes identified as overcast by the ERBE scene identification method (Wielicki and Green 1989) were averaged over different solar zenith, viewing zenith, and azimuth angular bins. The overcast visible radiances were used to retrieve cloud optical depths by using lookup tables of reflectances from radiative transfer calculations. The angular-bin averaged cloud optical depths were used to investigate their angular dependence. The retrieved cloud optical depths were also input to the broadband radiative transfer model to calculate SW reflectances. The model-computed SW reflectances were compared with the ScaRaB observations. The ScaRaB observed SW reflectances for the overcast scenes were used to derive a ScaRaB ADM, like the ERBE ADM. The two ADMs were compared for various solar zenith angles (SZA). The ADMs were also derived for both thick and thin overcast scenes and compared with the ADMs for the total overcast scenes. The thick and thin overcast scenes were determined by the percentile of visible reflectances stratified at each angle. Here, 75% to 95% in the visible reflectance is for the thick overcast scenes, while 5% to 25% is for the thin ones. By applying both the ERBE and ScaRaB ADMs to the SW reflectance measurements for angular conversion, the SW TOA albedos were derived and compared for total overcast and for thick and thin overcast scenes at different viewing directions.

In the radiative transfer calculations, an adding-doubling plane-parallel model was used together with the LOWTRAN7 model to account for the scattering and absorption by atmospheric molecules. A standard midlatitude summer atmosphere from McClatchey et al. (1972) was adopted. The atmosphere was divided into eight vertical layers with the cloud layer placed between 1 km and 2 km. Mie theory was used to calculate the absorption and scattering of cloud. Cloud droplets were assumed to be water sphere with an effective radius of 10 μm. Maritime aerosol properties were adopted from LOWTRAN7 with an optical depth of 0.1. Lambertian surface reflectance of 0.06 was used for all spectral wavelengths. In the model calculations, uncertainties were determined by changes of a factor of two in the atmospheric column water vapor and ozone, ±1 km in cloud top altitude, ±2 μm in droplet effective radius, 0 to 0.25 in aerosol optical depth, and 0 to 0.1 in surface reflectance.

Results

Cloud Optical Depth

Cloud optical depths retrieved from ScaRaB visible reflectances for the overcast scenes are shown in Figure 1 for two different SZAs. The retrieved cloud visible optical depths are plotted as a function of viewing zenith angle for eight relative azimuth angles, four of each in both the forward and backward scattering directions. The separation of the azimuth angles follows that used in the ERBE ADM. The dependence of cloud optical depth on the viewing angle is small for small SZA, but large for large SZA. The dependence is relatively small in the side and backward scattering directions for SZAs < 60°. In the forward direction, the cloud optical depth decreases with increasing viewing zenith angle at all SZAs. Figure 2 shows the dependence of cloud optical depth on SZA for different viewing directions. The cloud optical depth generally increases with SZA, except in the forward scattering direction. The increases in the side and backward scattering directions are relatively small for SZA < 60°.

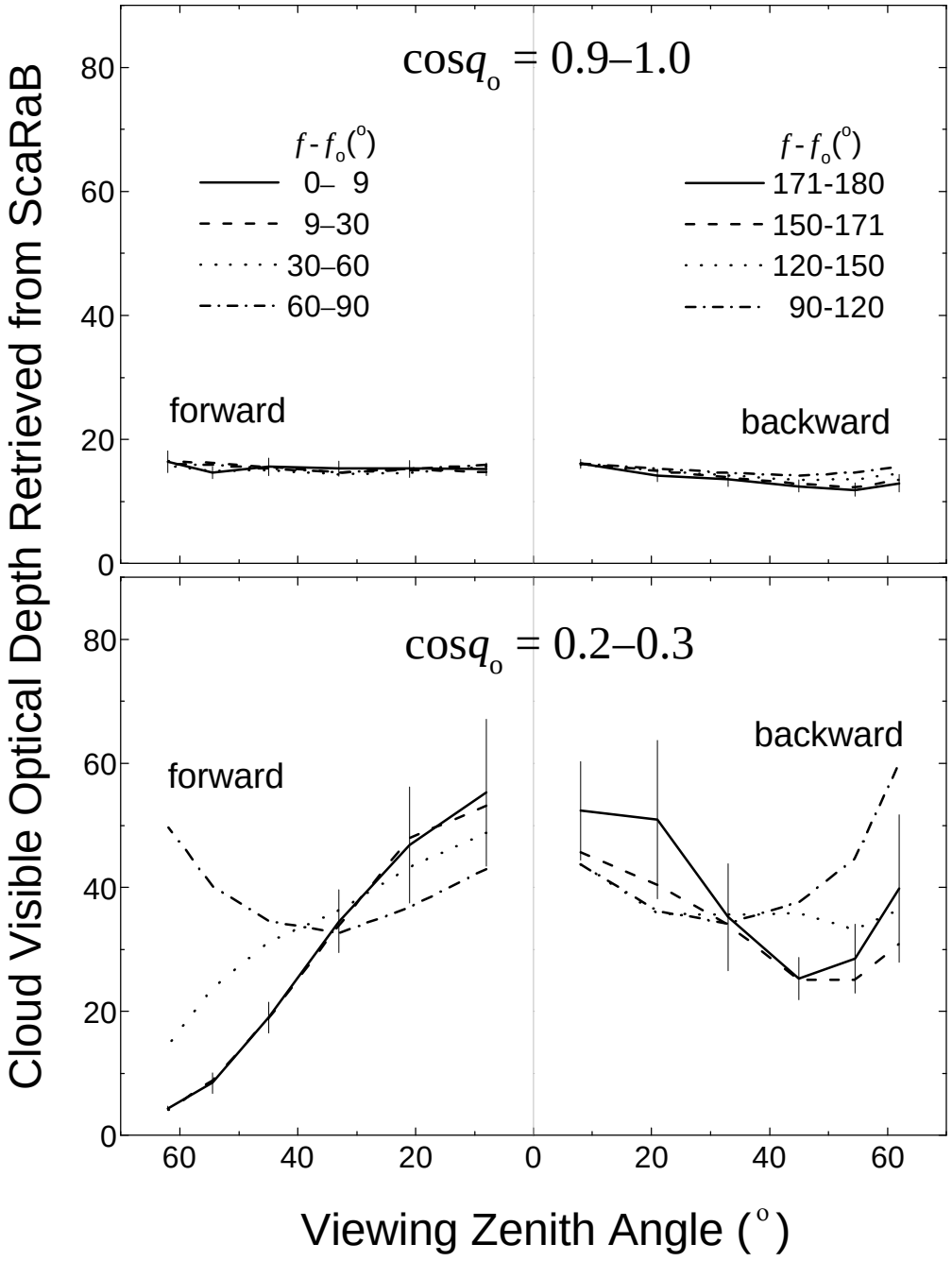

Figure 1. Angular-bin averaged cloud optical depth from one-year ScaRaB observations. The bar indicates the standard error of the mean.

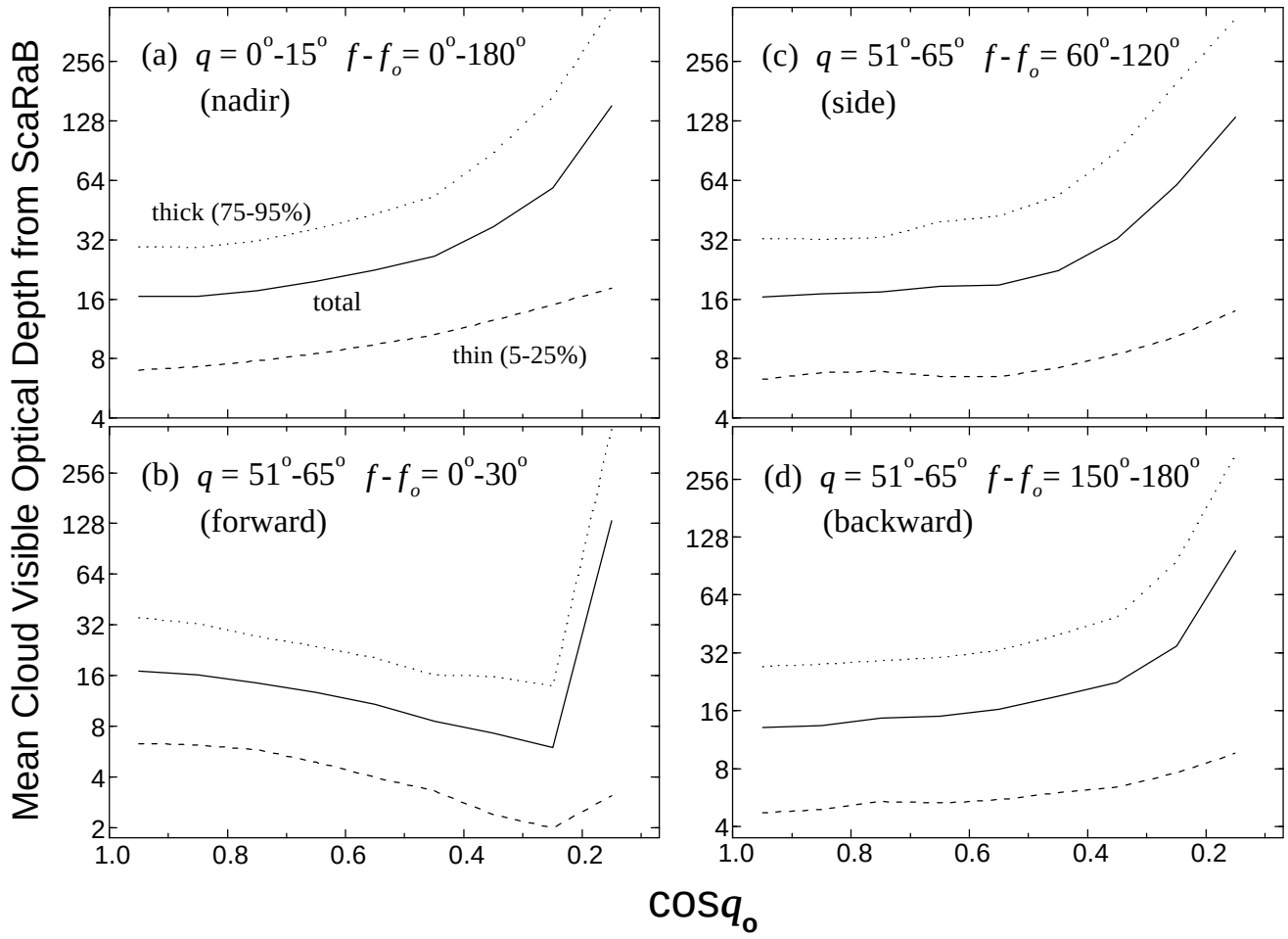

Figure 2. Mean cloud visible optical depths for different viewing directions. Results show for total overcast and for thick and thin overcast scenes.

Inversion of Visible to SW Reflectance

The SW overcast reflectances inverted using the cloud optical depth input to the broadband radiation model are compared with the ScaRaB observations. Figure 3 shows the comparisons for different viewing and scattering directions. The model-inverted SW reflectances are in good agreement with the ScaRaB observations for most viewing and scattering angles, except for the forward and backward scattering directions at large SZAs (> 60°). The underestimation in the model-inverted SW reflectances at large SZAs is due to that the plane-parallel model calculations had too much water vapor absorption above cloud. Since revealed from the ScaRaB 11-μm observations, these overcast scenes exhibit relatively cold temperatures (210K to 270K). The underestimation can be corrected by placing clouds at higher altitude.

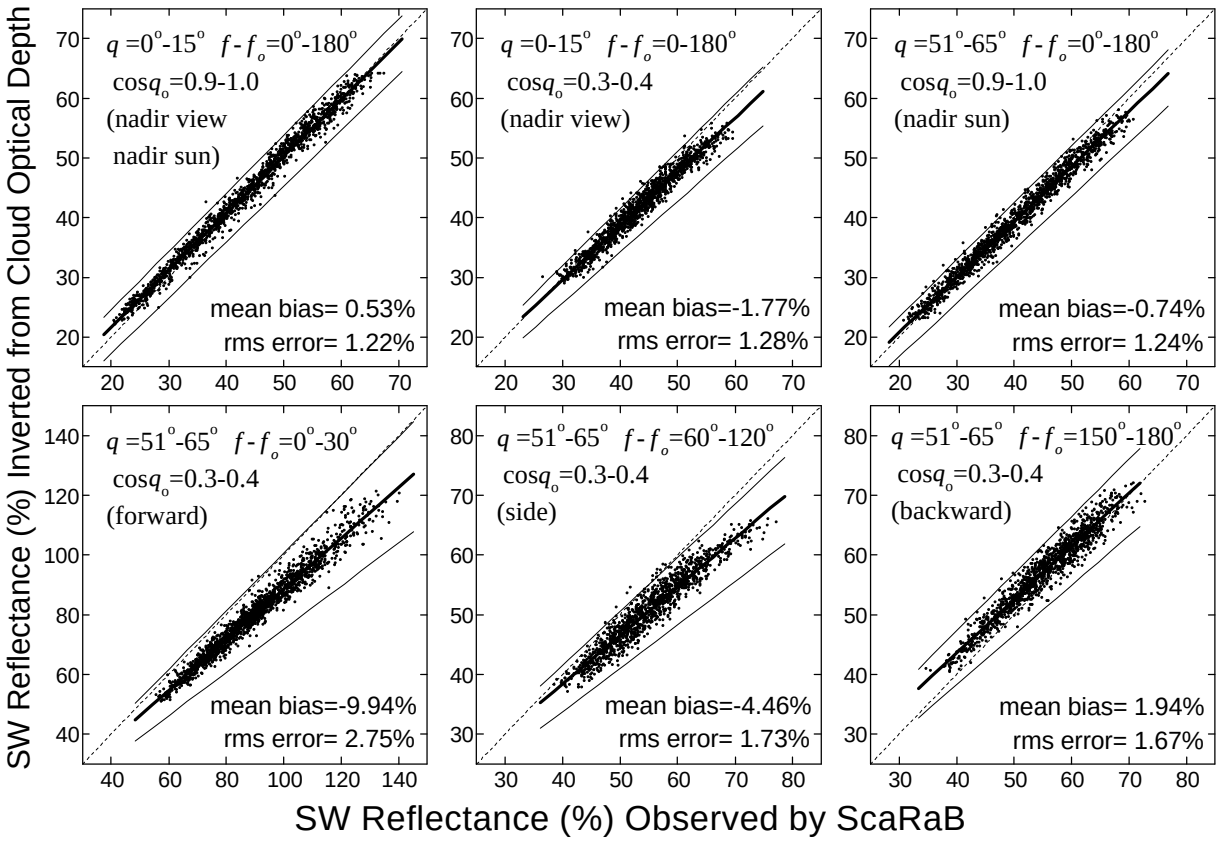

Figure 3. Comparisons of SW reflectances from model inversion and ScaRaB observation. The thick line is the least-squares fit to all data and the thin line shows its uncertainties.

Angular Correction and Albedo

Figure 4 compares the ADMs derived from ScaRaB SW reflectances with the ERBE ADMs for two different SZAs. The two ADMs generally agree well for all SZAs. The largest relative difference between the two is at certain backward scattering directions (~10%). The comparisons between the ScaRaB ADMs derived for total overcast scenes and for thick and thin overcast scenes are shown separately in Figure 5 (a, b). Figure 5a shows the ratio of thick to total overcast ADMs, while Figure 5b shows the ratio of thin to total overcast ADMs. Although the absolute differences are relatively larger for the thin-total comparison, the differences are generally within ±5%.

The SW TOA albedos derived by applying the ADMs to the ScaRaB SW reflectances are shown in Figure 6 for different viewing directions. The differences between the albedos derived using the ERBE ADMs and those with the ScaRaB ADMs are largest (~3%) in the backward scattering directions. For the thick and thin overcast scenes, the differences between albedos derived using ScaRaB total overcast ADM and those with thick and thin ADMs, respectively, are generally small.

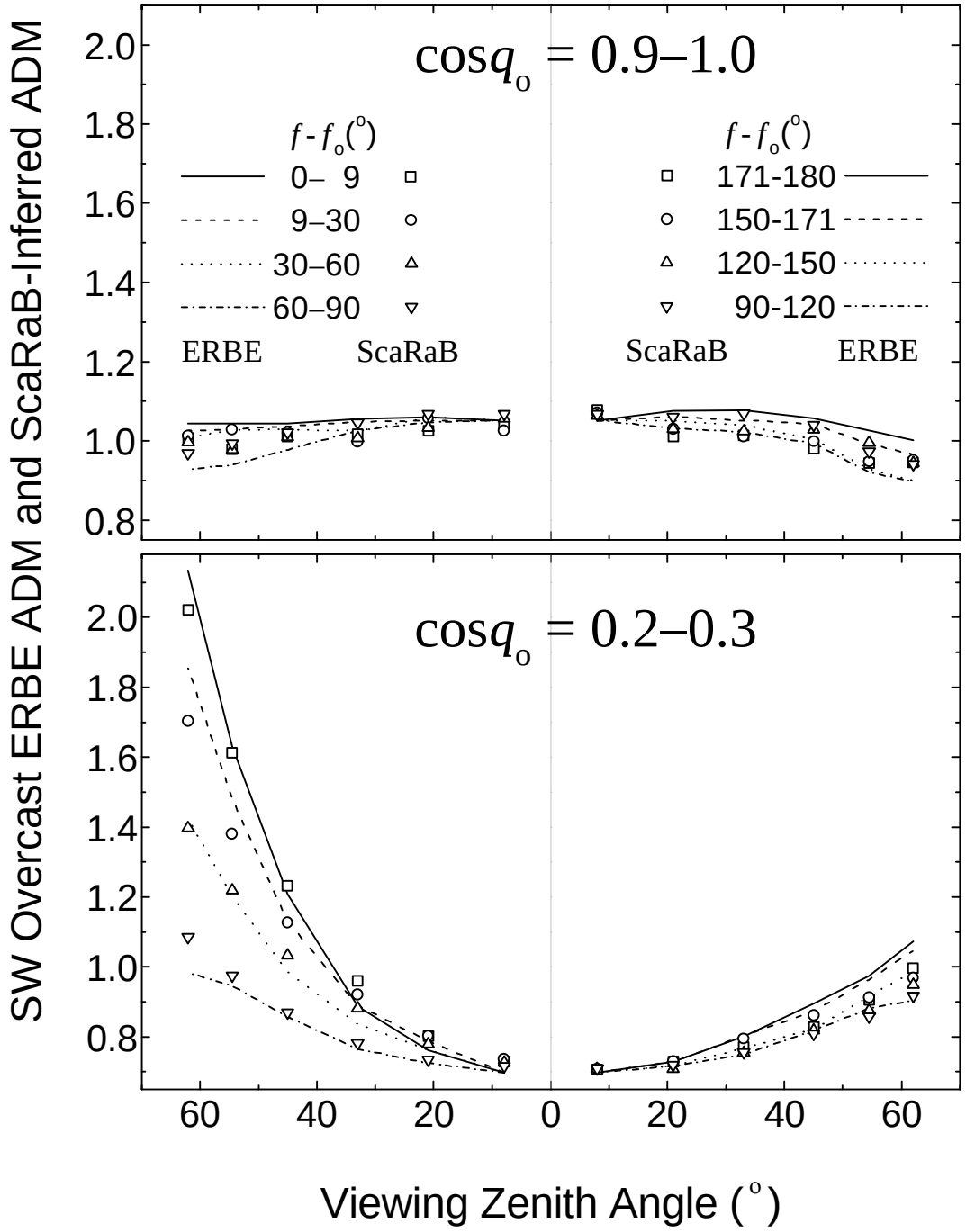

Figure 4. Comparison of the ScaRaB and ERBE ADMs.

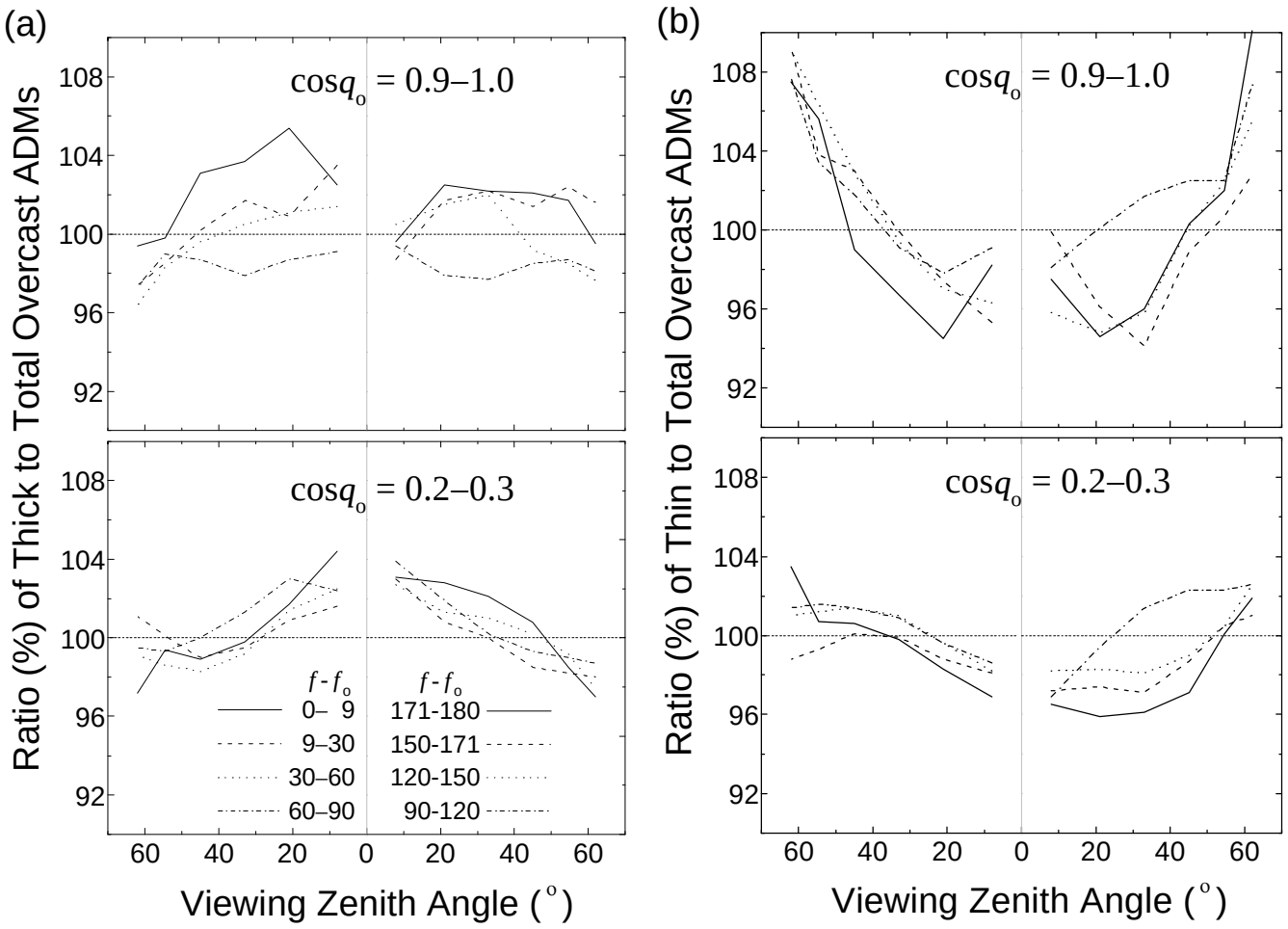

Figure 5. Ratio of the thick (a) and thin (b) overcast SW ADMs to average overcast ADM.

Summary

Cloud optical depths retrieved from ScaRaB overcast visible radiances show angular dependence on both SZA and viewing zenith angles. The cloud optical depth increases with SZA at nadir, but decreases in forward scattering direction (SZA < 75°). At side and backward scattering directions, the cloud optical depth remains relatively stable for SZA < 60°. Using plane-parallel cloud optical depths, the model-inverted SW reflectances show reasonable agreement with the ScaRaB observations, provided the atmospheric data and cloud elevation are known.

The SW overcast ADMs inferred from ScaRaB observations show generally good agreement with the ERBE ADMs. The relative difference was largest in the back scattering direction. The ADMs inferred for thick or thin overcast clouds were within ±5% of the total overcast ADM for most viewing and scattering angles. When averaged over all viewing angles, SW TOA albedos derived using ScaRaB ADMs agree well with those derived with ERBE ADMs. But, the difference can be large (> 3%) at certain viewing directions.

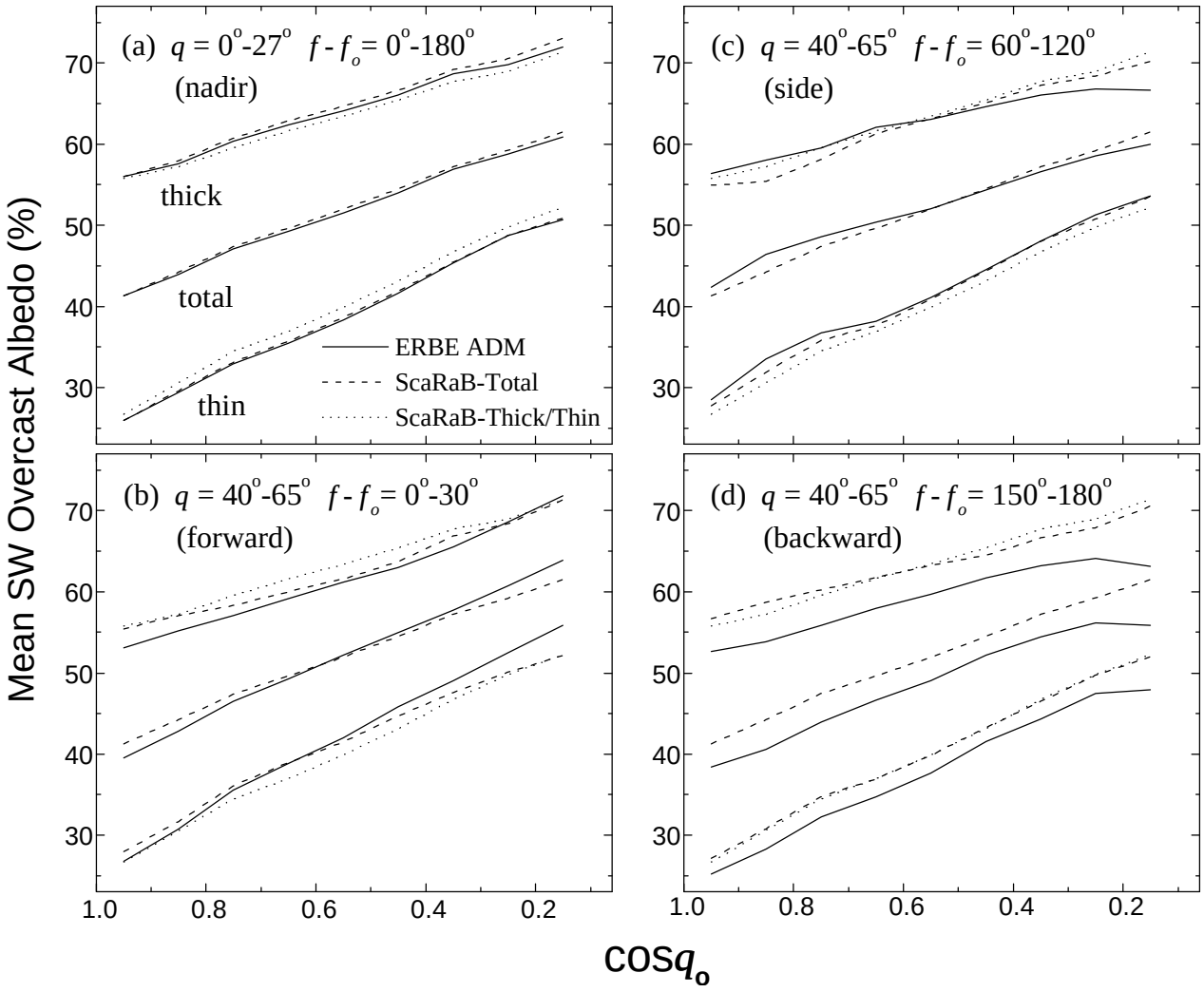

Figure 6. Mean SW TOA albedos derived for thin, thick, and total overcast scenes for four different scattering/viewing directions.

Acknowledgment

This work was supported by Research Grant No. DE-FG02-97ER62361, from U.S. Department of Energy.

References

Cess, R. D., and G. L. Potter, 1986: Narrow- and broadband satellite measurements of shortwave radiation: Conversion simulations with a general circulation model. *J. Climate Appl. Meteorol.*, **25**, 1977-1984.

Kandel, R., et al., 1998: The ScaRaB earth radiation budget dataset. *Bull. Amer. Meteorol. Soc.*, **79**, 765-783.

McClatchey, R. A., R. W. Fenn, J. E. Selby, F. E. Volz, and J. S. Garing, 1972: *Optical properties of the atmosphere.* Air Force Cambridge Research Laboratories. AFCRL-72-0497, No. 411, 108 pp.

Rossow, W. B., and R. A. Schiffer, 1991: ISCCP cloud data products. *Bull. Amer. Meteorol. Soc.*, **72**, 2-20.

Suttles, J. T., et al., 1988: Angular radiation models for Earth-atmosphere system. Vol. I-Shortwave radiation. *NASA Refer. Publ.*, 1,184, 144 pp.

Wielicki, B. A., B. R. Barkstrom, E. F. Harrison, R. B. Lee, III, G. L. Smith, and J. E. Cooper, 1996: Cloud and the Earth Radiant Energy System (CERES): An Earth Observing System experiment. *Bull. Amer. Meteorol. Soc.*, **77**, 853-868.

Wielicki, B. A., R. D. Cess, M. D. King, D. A. Randall, and E. F. Harrison, 1995: Mission to planet earth: Role of clouds and radiation in climate. *Bull. Amer. Meteorol. Soc.*, **76**, 2125-2153.

Wielicki, B. A., and R. N. Green, 1989: Cloud identification for ERBE radiative flux retrieval. *J. Appl. Meteorol.*, **28**, 1133-1146.